INTERNATIONAL JOURNAL FOR NUMERICAL METHODS IN FLUIDS, VOL. 8, 579–597 (1988)

LAMINAR FLOW AND HEAT TRANSFER IN A PERIODICALLY CONVERGING–DIVERGING CHANNEL

VIJAY K. GARG*

Department of Mechanical Engineering, The Ohio State University, Columbus, Ohio 43210, U.S.A.

AND

P. K. MAJI

Durgapur Steel Plant, Durgapur, India

SUMMARY

A finite difference solution for laminar viscous flow through a sinusoidally curved converging–diverging channel is presented. The physical wavy domain is transformed into a rectangular computational domain in order to simplify the application of boundary conditions on the channel walls. The discretized conservation equations for mass, momentum and energy are derived on a control volume basis. The pseudo-diffusive terms that arise from the co-ordinate transformation are treated as source terms, and the resulting system of equations is solved by a semi-implicit procedure based on line relaxation. Results are obtained for both the developing and the fully developed flow for a Prandtl number of 0·72, channel maximum width-to-pitch ratio of 1·0, Reynolds number ranging from 100 to 500 and wall amplitude-to-pitch ratio varying from 0·1 to 0·25. Results are presented here for constant fluid properties and for a prescribed wall enthalpy only.

KEY WORDS

INTRODUCTION

Viscous fluid flow past a wavy boundary has attracted considerable interest due to its application in different areas such as generation of wind waves on water, formation of sedimentary ripples in river channels and dunes in deserts, transpiration cooling of re-entry vehicles and rocket boosters, cross-hatching on ablative surfaces and film vaporization in combustion chambers. Such a configuration is also used in heat exchangers in order to enhance the convective heat transfer characteristics of the device.

Viscous flow in sinusoidally varying channels and pipes was first treated by Burns and Parks.[1] They carried out the solution by expressing the stream function in a Fourier cosine series under the assumption that both wall amplitude and Reynolds number are small enough for the Stokes approximation to be valid. Tsangaris and Leiter[2] solved the same problem by expressing the stream function in a Fourier series not in the physical plane but in the transformed plane, where the wavy boundary is transformed into a straight one. This analytical perturbation method for creeping flow was later extended to laminar flow for higher Reynolds numbers by the same authors.[3]

* On sabbatical leave from Indian Institute of Technology, Kanpur, India.

0271–2091/88/050579–19$09.50

Received 30 April 1987
Revised 4 August 1987

However, their analysis is valid only for very small wall amplitude-to-pitch ratio. Fluid flow connected with heat transfer in wavy channels was calculated by Vajravelu[4] by the perturbation method for long-wavelength channels. The heat transfer effect has also been studied by Prata and Sparrow[5] for fully developed laminar flow in an annular duct having a streamwise periodic variation of the cross-sectional area. They obtained the solution by using the SIMPLE algorithm of Patankar.[6] Some experimental work has also been carried out by Hsu and Kennedy[7] to find the variation of pressure and shear stress along a wavy pipe for turbulent non-separated flow.

In the present work a finite difference approach for the solution of two-dimensional, viscous laminar flow in sinusoidally varying symmetric channels is presented. There is no limitation to the ratio of wall amplitude to pitch. The discretized conservation equations are derived on a control volume basis.[8] The resulting discretized equations are solved using the SIMPLEC method suggested by Van Doormaal and Raithby.[9] Their other suggestions regarding the use of an E-factor in place of the usual under-relaxation factor and the solution of the pressure correction equation are also adopted here. This reduces the solution cost considerably.

FORMULATION OF THE PROBLEM

A schematic view of the physical domain being considered is shown in Figure 1 (for the first cycle only). The walls of the channel are defined by a function $\delta'(x)$ given by

$$\delta'(x) = L - \lambda[1 + \cos(\pi x/L_c)], \tag{1}$$

where $2L$ is the maximum width of the channel, 2λ is the amplitude of the channel walls and $2L_c$ is the pitch of the wavy boundary. The origin of the co-ordinate system is placed on the entrance plane of the duct as shown in Figure 1.

The governing equations to be considered here are the continuity, momentum and energy equations. Constant thermophysical properties are assumed and viscous dissipation is neglected in the energy equation. Only forced convection is considered and the channel is taken to be isothermal and horizontal. Moreover, the flow is considered two-dimensional. Using these assumptions and the dimensionless variables

$$X = x/L_c, \qquad Y = y/L_c, \qquad U = u/U_0, \qquad V = v/U_0,$$
$$P = (p - p_0)/(\rho U_0^2), \qquad H = (h - h_w)/(h_0 - h_w),$$

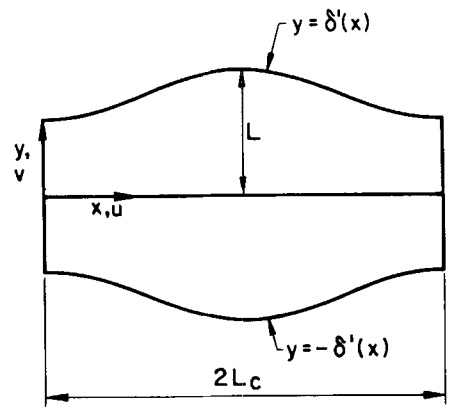

Figure 1. Converging–diverging channel

where U_0, p_0 and h_0 are the uniform velocity, pressure and enthalpy at the entrance to the channel and h_w is the uniform enthalpy at the wall, the governing equations take the form

$$\frac{\partial U}{\partial X}+\frac{\partial V}{\partial Y}=0, \tag{2}$$

$$U\frac{\partial U}{\partial X}+V\frac{\partial U}{\partial Y}=-\frac{\partial P}{\partial X}+\frac{1}{Re}\left(\frac{\partial^2 U}{\partial X^2}+\frac{\partial^2 U}{\partial Y^2}\right), \tag{3}$$

$$U\frac{\partial V}{\partial X}+V\frac{\partial V}{\partial Y}=-\frac{\partial P}{\partial Y}+\frac{1}{Re}\left(\frac{\partial^2 V}{\partial X^2}+\frac{\partial^2 V}{\partial Y^2}\right), \tag{4}$$

$$U\frac{\partial H}{\partial X}+V\frac{\partial H}{\partial Y}=\frac{1}{Pe}\left(\frac{\partial^2 H}{\partial X^2}+\frac{\partial^2 H}{\partial Y^2}\right), \tag{5}$$

where $Re=\rho U_0 L_c/\mu$ is the Reynolds number and $Pe=RePr$ is the Peclet number, with $Pr=\mu C_p/k$ the Prandtl number and ρ, μ, k and C_p the density, dynamic viscosity, thermal conductivity and specific heat at constant pressure respectively for the fluid. Due to symmetry about the channel centreline, we need to consider only half of the channel. Thus the boundary conditions are

$$\begin{aligned}
&U(0,Y)=1, \qquad P(0,Y)=0, \qquad H(0,Y)=1,\\
&U(X,\delta(X)/2)=0, \qquad V(X,\delta(X)/2)=0, \qquad H(X,\delta(X)/2)=0,\\
&\partial U(X,0)/\partial Y=0, \qquad V(X,0)=0, \qquad \partial H(X,0)/\partial Y=0,\\
&U(X^*,Y)=U[(X^*+2),Y], \qquad V(X^*,Y)=V[(X^*+2),Y],\\
&H(X^*,Y)/H[(X^*+2),Y]=H[(X^*+2),Y]/H[(X^*+4),Y],
\end{aligned} \tag{6}$$

where X^* is an arbitrary location in the fully developed region and $\delta(X)=2\delta'(X)/L_c$. The last three boundary conditions in equations (6) imply periodic nature of the fully developed flow. For the isothermal wall condition the cross-sectional shape of the enthalpy difference $[H(X,Y)-H_w]$ repeats itself periodically in the fully developed region, but the level decreases in the streamwise direction.[5] In fact the ratio H/H_b, where H_b is the dimensionless bulk enthalpy defined later in equation (16), is constant in the fully developed region. This leads to the last boundary condition in equations (6).

The next step in the analysis is to introduce a transformation of co-ordinates in order to transform the wavy physical domain into a rectangular computational domain so as to simplify the application of boundary conditions at the wall. This is done by the relations

$$\eta=X, \qquad \xi=Y/\delta(X) \tag{7}$$

such that $\xi=\pm 0{\cdot}5$ at all points on the curved boundaries.

The lines of constant η and ξ for a given shape are illustrated in Figure 2. It is evident that a control volume contained between lines $\eta=\eta_1$, $\eta=\eta_2$ and $\xi=\xi_1$, $\xi=\xi_2$ is a curvilinear element with non-orthogonal sides. The quantities $\mathbf{e}_\eta$ and $\mathbf{e}_\xi$ are unit vectors in the physical co-ordinate system which lie along the lines of constant ξ and constant η respectively. It is evident from the figure that the direction of $\mathbf{e}_\eta$ changes with position whereas the unit vectors $\mathbf{e}_X$ and $\mathbf{e}_Y$ do not change direction throughout the solution domain. We also note that $\mathbf{n}$, the unit vector normal to the ξ-constant lines, is given by

$$\mathbf{n}=\nabla\xi/|\nabla\xi|=\alpha^{-1/2}(\mathbf{e}_Y-\beta\mathbf{e}_X), \tag{8}$$

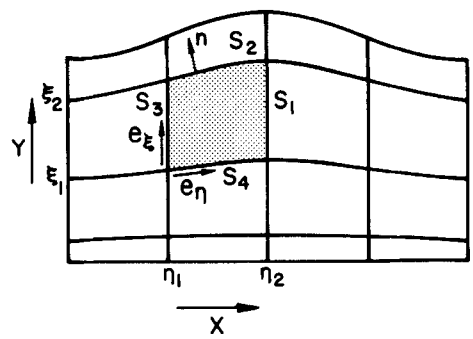

Figure 2. Shape of control volume in physical space

where

$$\beta = \xi \, \mathrm{d}\delta/\mathrm{d}\eta, \qquad \alpha = 1 + \beta^2.$$

In order to resolve the vector momentum equation (of which equations (3) and (4) are the two components) along the η, ξ directions, the unit vectors $\mathbf{e}_\eta$ and $\mathbf{e}_\xi$ illustrated in Figure 2 are used. Since the lines of constant η coincide with the lines parallel to the y-co-ordinate, we have

$$\mathbf{e}_\xi = \mathbf{e}_Y.$$

Since the unit vector $\mathbf{e}_\eta$ is perpendicular to the vector $\mathbf{n}$, we have

$$\mathbf{e}_\eta \cdot \mathbf{n} = 0,$$

which yields

$$\mathbf{e}_\eta = \alpha^{-1/2}(\mathbf{e}_X + \beta \mathbf{e}_Y). \tag{9}$$

Thus the unit vector $\mathbf{e}_\eta$ is a function of position. The following inverse relations can be obtained directly from equation (9):

$$\mathbf{e}_X = \alpha^{1/2}\mathbf{e}_\eta - \beta \mathbf{e}_\xi, \qquad \mathbf{e}_Y = \mathbf{e}_\xi. \tag{10}$$

The velocity vector $\mathbf{W}$ can be expressed as

$$\mathbf{W} = U\mathbf{e}_X + V\mathbf{e}_Y = U_\eta \mathbf{e}_\eta + U_\xi \mathbf{e}_\xi,$$

so that

$$U_\eta = \alpha^{1/2} U, \qquad U_\xi = V - \beta U. \tag{11}$$

Substituting $\mathbf{e}_X$ and $\mathbf{e}_Y$ from equation (10) into the vector momentum equation, then collecting the coefficients of unit vectors $\mathbf{e}_\eta$ and $\mathbf{e}_\xi$ and finally using $U_\xi = V - \beta U$, we find that (a) the momentum equation in the η-direction is the same as equation (3) and (b) the momentum equation in the ξ-direction becomes

$$U\frac{\partial U_\xi}{\partial X} + V\frac{\partial U_\xi}{\partial Y} = \beta\frac{\partial P}{\partial X} - \frac{\partial P}{\partial Y} + \frac{1}{Re}\left(\frac{\partial^2 U_\xi}{\partial X^2} + \frac{\partial^2 U_\xi}{\partial Y^2}\right) - U\left(U\frac{\partial \beta}{\partial X} + V\frac{\partial \beta}{\partial Y}\right)$$
$$+ \frac{U}{Re}\left(\frac{\partial^2 \beta}{\partial X^2} + \frac{\partial^2 \beta}{\partial Y^2}\right) + \frac{2}{Re}\left(\frac{\partial U}{\partial X}\frac{\partial \beta}{\partial X} + \frac{\partial U}{\partial Y}\frac{\partial \beta}{\partial Y}\right). \tag{12}$$

Thus the velocity components solved for are U and U_ξ. It turns out that the momentum equation (3) for the velocity component U is much simpler than the transformed version having U_η as the dependent variable. On the other hand, the form of momentum equation (12) is attractive since it displays U_ξ as the primary dependent variable instead of the clumsy combination of U and V that appears in the convective and diffusive terms of the transformed version of equation (4).

The continuity and energy equations are scalars and remain as they are. The boundary conditions are

$$\begin{aligned}
&U(0,\xi)=1, \qquad P(0,\xi)=0, \qquad H(0,\xi)=1,\\
&U(\eta,0{\cdot}5)=0, \qquad U_\xi(\eta,0{\cdot}5)=0, \qquad H(\eta,0{\cdot}5)=0,\\
&\partial U(\eta,0)/\partial\xi=0, \qquad U_\xi(\eta,0)=0, \qquad \partial H(\eta,0)/\partial\xi=0,\\
&U(\eta^*,\xi)=U[(\eta^*+2),\xi], \qquad U_\xi(\eta^*,\xi)=U_\xi[(\eta^*+2),\xi],\\
&H(\eta^*,\xi)/H[(\eta^*+2),\xi]=H[(\eta^*+2),\xi]/H[(\eta^*+4),\xi],
\end{aligned} \tag{13}$$

where $\eta^* = X^*$.

Nusselt number

The local Nusselt number, based on twice the mean width, $4(L-\lambda)$, of the channel, can be written as

$$Nu = 4(L-\lambda)h_t/k, \tag{14}$$

where h_t is the heat transfer coefficient given by

$$h_t = \frac{-k(\partial h/\partial n)|_{y=\delta'(x)}}{h_b - h_w} \tag{15}$$

The bulk enthalpy h_b is given by

$$h_b = \int_0^{\delta'(x)} uh\,dy \Big/ \int_0^{\delta'(x)} u\,dy$$

or, in dimensionless form, by

$$H_b = \int_0^{\delta(X)/2} UH\,dY \Big/ \int_0^{\delta(X)/2} U\,dY. \tag{16}$$

Since $\xi = Y/\delta(X)$, and H_b is a function of X alone, we get at any location X

$$H_b(X) = \int_0^{1/2} \delta(X)UH\,d\xi \Big/ \int_0^{1/2} \delta(X)U\,d\xi = 2\frac{\delta(X)}{\delta(0)}\int_0^{1/2} UH\,d\xi. \tag{17}$$

At axial locations where $\beta = 0$ we have $\partial/\partial n = \partial/\partial y$. Such locations have $\eta = 0, 1, 2, \ldots$. At these locations the Nusselt number is given by

$$Nu = -4(L-\lambda)(\partial H/\partial\xi)_{\xi=0{\cdot}5}/(H_b\delta L_c). \tag{18}$$

Control volume form of the conservation equations

Using the divergence theorem the governing equations (equations (2), (3), (12) and (5)) are integrated over a control volume bounded by lines of constant η and constant ξ as shown in

Figure 2. This is done with a view to obtaining the discretization equations. Equations obtained in this manner express the conservation principle for the dependent variable over the finite control volume, just as the differential equation expresses it for an infinitesimal control volume. The resulting equations are:

Continuity equation

$$\int_S (\mathbf{W}\cdot\mathbf{n})\,\mathrm{d}S = 0, \tag{19}$$

η-momentum equation

$$\int_S (\mathbf{W}\cdot\mathbf{n})U\,\mathrm{d}S - Re^{-1}\int_S (\mathbf{n}\cdot\nabla U)\,\mathrm{d}S = -\int_{\mathcal{V}} (\partial P/\partial X)\,\mathrm{d}\mathcal{V}, \tag{20}$$

ξ-momentum equation

$$\int_S (\mathbf{W}\cdot\mathbf{n})U_\xi \mathrm{d}S - Re^{-1}\int_S (\mathbf{n}\cdot\nabla U_\xi)\,\mathrm{d}S$$
$$= \int_{\mathcal{V}} (\beta\partial P/\partial X - \partial P/\partial Y)\,\mathrm{d}\mathcal{V} - \int_{\mathcal{V}} U(\mathbf{W}\cdot\nabla\beta)\,\mathrm{d}\mathcal{V} + Re^{-1}\int_{\mathcal{V}} [U\nabla^2\beta + 2\nabla U\cdot\nabla\beta]\,\mathrm{d}\mathcal{V}, \tag{21}$$

energy equation

$$\int_S (\mathbf{W}\cdot\mathbf{n})H\,\mathrm{d}S - Pe^{-1}\int_S (\mathbf{n}\cdot\nabla H)\,\mathrm{d}S = 0, \tag{22}$$

where $\mathcal{V}$ and S represent respectively the dimensionless volume and surface of the control volume. Also vector notation is used to keep the equations in a compact form.

In the next step the above surface integrals are subdivided into a sum of four surface integrals over the segments S_1, S_2, S_3 and S_4. Then the quantities $\mathrm{d}S$ and $\mathbf{n}$ for each surface are evaluated. For example, for surface S_1, unit normal vector $\mathbf{n}=\mathbf{e}_X$ and $\mathrm{d}S=\xi\mathrm{d}\xi$, while for surface S_2, $\mathbf{n}=\alpha^{-1/2}(-\beta\mathbf{e}_X+\mathbf{e}_Y)$ and $\mathrm{d}S=\alpha^{1/2}\mathrm{d}\eta$. It is obvious that for surfaces S_3 and S_4 all the quantities are identical to those for surfaces S_1 and S_2, with the exception that the outward normal $\mathbf{n}$ has the opposite sign. It is also necessary to consider a formal transformation between derivatives with respect to X, Y and those with respect to η, ξ. This transformation is

$$\partial/\partial X = \partial/\partial\eta - (\beta/\delta)\partial/\partial\xi, \qquad \partial/\partial Y = (1/\delta)\partial/\partial\xi. \tag{23}$$

Also for evaluating the volume integrals in equation (20) and (21), we note that $\mathrm{d}\mathcal{V}=\delta\,\mathrm{d}\eta\,\mathrm{d}\xi$. Finally equations (20), (21) and (22) can be expressed in a common compact form as

$$\int_{S_1} [U\phi\delta + \Gamma(\gamma+\psi)]\mathrm{d}\xi - \int_{S_3} [U\phi\delta + \Gamma(\gamma+\psi)]\,\mathrm{d}\xi$$
$$+ \int_{S_2} [U_\xi\phi + \Gamma(\Omega+\Lambda)]\,\mathrm{d}\eta - \int_{S_4} [U_\xi\phi + \Gamma(\Omega+\Lambda)]\,\mathrm{d}\eta = b, \tag{24}$$

where ϕ stands for U, U_ξ or H, $\Gamma = 1/Re$ for the momentum equations, $\Gamma = 1/Pe$ for the energy equation and

$$\Omega = -(\alpha/\delta)\,\partial\phi/\partial\xi, \qquad \gamma = -\delta\,\partial\phi/\partial\eta,$$
$$\psi = \beta\,\partial\phi/\partial\xi, \qquad \Lambda = \beta\,\partial\phi/\partial\eta.$$

For the η-momentum equation, b is given by

$$b = -\int_{\nu} [\partial P/\partial \eta - (\beta/\delta)\partial P/\partial \xi]\delta \, d\eta \, d\xi.$$

For the ξ-momentum equation, b is given by

$$b = \int_{\nu} \left(\beta \frac{\partial P}{\partial \eta} - \frac{\alpha}{\delta}\frac{\partial P}{\partial \xi}\right)\delta \, d\eta \, d\xi - \int_{\nu} U\left(\frac{U_\xi}{\delta}\frac{d\delta}{d\eta} + \xi U \frac{d^2\delta}{d\eta^2}\right)\delta \, d\eta \, d\xi$$
$$+ \frac{1}{Re}\int_{\nu} U\left[\xi \frac{d^3\delta}{d\eta^3} + \frac{2\xi}{\delta^2}\left(\frac{d\delta}{d\eta}\right)^3 - \frac{3\xi}{\delta}\frac{d\delta}{d\eta}\frac{d^2\delta}{d\eta^2}\right]\delta \, d\eta \, d\xi$$
$$+ \frac{2}{Re}\int_{\nu}\left[\frac{\partial U}{\partial \eta}\left(\xi \frac{d^2\delta}{d\eta^2} - \frac{\beta}{\delta}\frac{d\delta}{d\eta}\right) + \frac{\partial U}{\partial \xi}\left(\frac{\alpha}{\delta^2}\frac{d\delta}{d\eta} - \frac{\beta\xi}{\delta}\frac{d^2\delta}{d\eta^2}\right)\right]\delta \, d\eta \, d\xi.$$

For the energy equation, b is simply zero.

Finally the continuity equation (19) can be written as

$$\int_{S_1} U\delta \, d\xi + \int_{S_2} U_\xi \, d\eta - \int_{S_3} U\delta \, d\xi - \int_{S_4} U_\xi \, d\eta = 0. \tag{25}$$

If velocities are retained in terms of physical components U and V, the resulting continuity equation will involve two extra mass flux terms on the surfaces S_2 and S_4.

FINITE DIFFERENCE FORMULATION AND NUMERICAL SOLUTION

Domain discretization

For the derivation of finite difference equations the rectangular computational domain in the η, ξ co-ordinate system is first discretized by placing grid points at the geometric centres of the control volumes drawn in an arbitrary non-uniform manner. In this practice a control volume face is not midway between adjacent grid points. This yields a less accurate finite difference representation of the derivatives. However, this practice has merits in that (i) the grid point at the centre of the control volume well represents the control volume and (ii) discontinuities in thermophysical properties, boundary conditions and sources are more readily accomodated.

If the pressure and velocities are computed at the same locations, and if linear interpolation are used to evaluate them at the control volume faces, unrealistic velocity fields can arise as a solution (Reference 6, pp. 115–120). A remedy for this is to calculate velocities and pressure at different locations. Thus the velocity grid points are displaced in some way from those of the pressure. The locations where pressure and other scalar dependent variables such as enthalpy are calculated are designated as main grid points. The control volumes for the velocity component U are staggered horizontally while those for the velocity component U_ξ are staggered vertically with respect to the main control volumes. This staggering is done in such a way that the displaced faces pass through the main grid points while non-displaced faces lie along the main control volume faces. Hence the resultant shape of the control volume used to compute velocity components and other dependent variables becomes L-shaped, as shown in Figure 3. In this figure the main grid points are denoted by dots identified by letters P, W, E, S, N, SW, SE, NW and NE, whereas U-velocity locations are denoted by arrows ($\times\!\!\rightarrow$) identified by P″, W″, E″, S″, N″, SW″, SE″, NW″ and NE″ and U_ξ-velocity locations are denoted by arrows ($\overset{\uparrow}{\times}$) identified by P′, W′, E′, S′, N′, SW′, SE′, NW′ and NE′. In the same figure the main control volume and the control volumes for velocity components U and U_ξ

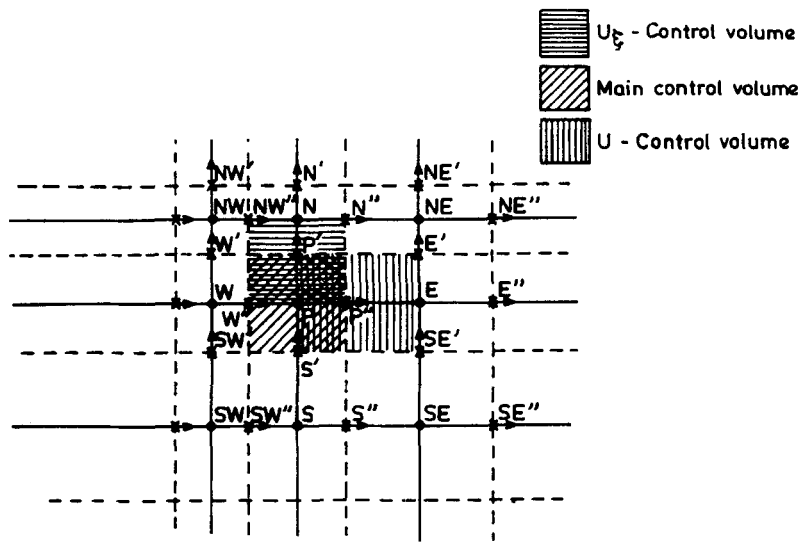

Figure 3. Type of control volume considered

are identified by inclined, vertical and horizontal hatch lines respectively. The type of control volume used for velocities near the boundary is different, as shown in Figure 4. The various geometrical quantities needed for discretizing the governing equations are also shown in Figures 3 and 4.

Discretization of the governing equations

The choice of a particular scheme for discretization of the governing equations depends upon the relative importance of convection and diffusion. When convection is small, central differencing can be used to yield results of high accuracy for a suitably small mesh size. However, for fluid flow problems in general convection may be large. Therefore the scheme should account for the special influence of the upstream points. Patankar[6] points out that for the one-dimensional convection–diffusion problem the exponential scheme provides exact results. While this scheme is time-consuming, an efficient scheme that closely approximates the exponential one is the power-

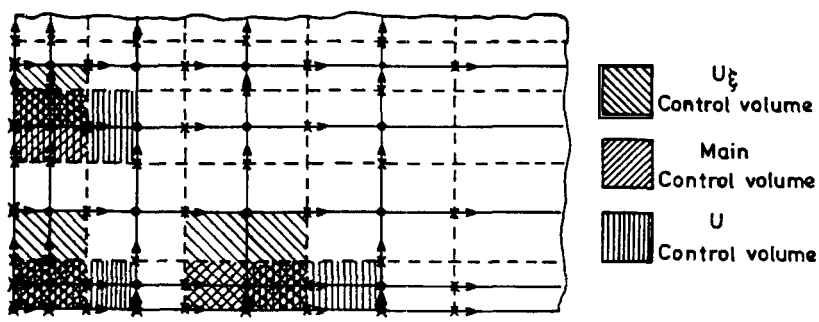

Figure 4. Type of control volume at the boundary

law scheme.[6] This is the scheme used here. Details of the method for discretization of equation (24) for various values of ϕ are given in Reference 8 and will not be repeated here. The result is

$$(a_m - S_m)\phi_m = \sum a_{nb}\phi_{nb} + S_{\phi m}, \tag{26}$$

where the subscript m indicates the value at the point P″, P′ or P respectively for the U-momentum, U_ξ-momentum or energy equation, subscript nb represents the value at the neighbour points in east, west, north and south directions, coefficient a includes both convective and diffusive contributions and S is the linearized source term containing the pseudo-diffusive contributions due to co-ordinate transformation. Note that S_m vanishes for the U-momentum and energy equations but not for the U_ξ-momentum equation.

Discretization of the continuity equation

The control volume of specific interest in this case is that which surrounds the main grid point P in Figure 3. The surface integrals in equation (25) are now approximated by evaluating the integrand at points, e, n, w and s respectively. Then the integration is performed by regarding these values as constant over each face to obtain

$$U_{P''}\delta_e\Delta\xi + (U_\xi)_{P'}\Delta\eta - U_{W''}\delta_w\Delta\xi - (U_\xi)_{S'}\Delta\eta = 0, \tag{27}$$

where $\Delta\eta$ and $\Delta\xi$ denote the size of the main control volume in the η and ξ directions respectively.

Under-relaxation factor

Equation (26) is non-linear since its coefficients depend upon one or more of the dependent variables represented by ϕ. To account for the resulting inter-equation linkages and non-linearities, repeated solutions of the nominally linear form of equation (26) are required. In order to moderate the changes in successive solutions for ϕ, and thereby improve convergence, under-relaxation is used.

Van Doormaal and Raithby[9] introduce under-relaxation through the use of an E-factor as follows:

$$D_m\phi_m = \sum a_{nb}\phi_{nb} + S_{\phi m} + (1/E)(a_m - S_m)\phi_m^0, \tag{28}$$

where

$$D_m = (a_m - S_m)(1 + 1/E)$$

and ϕ_m^0 is the value of ϕ_m from the previous iteration. In order to accelerate convergence, values of E well in excess of unity are desirable. In fact values of E in the range 2–16 were found to be useful for the present problem. It may be pointed out that for calculations in body-fitted co-ordinates an iterative method is better than direct solution methods.[10]

Derivation of the pressure correction equation

We use the SIMPLEC procedure[9] for handling the velocity–pressure linkages. In this method the pressure field is first guessed. With this guessed pressure field, coefficients of the momentum equations can be evaluated allowing these equations to be solved to obtain the flow field. In general this flow field does not satisfy the continuity equation (27). Therefore this guessed pressure field is corrected so that the resulting velocity field satisfies the continuity equation. This is accomplished by the pressure correction equation which is derived[9] by combining the continuity equation with truncated forms of the momentum equations. After solving the pressure correction equation

following the recommendation given in Reference 9, the velocity and pressure fields are corrected and the procedure is repeated until the flow field satisfies both the continuity and momentum equations.

The final form of the pressure correction equation becomes

$$a_P P'_P = a_E P'_E + a_W P'_W + a_N P'_N + a_S P'_S + B, \tag{29}$$

where

$$a_E = d_{P''}\delta_{P''}\Delta\xi, \qquad a_W = d_{W''}\delta_{W''}\Delta\xi,$$
$$a_N = d_{P'}\Delta\eta, \qquad a_S = d_{S'}\Delta\eta,$$
$$a_P = a_E + a_W + a_N + a_S$$

and

$$B = -(U^*_\xi)_{P'}\Delta\eta + (U^*_\xi)_{S'}\Delta\eta - (U^*\delta)_{P''}\Delta\xi + (U^*\delta)_{W''}\Delta\xi,$$

with $d_{P''}$, $d_{W''}$, $d_{P'}$ and $d_{S'}$ given by

$$d_{P''} = \delta_{P''}\Delta\xi/(D_{P''} - \sum a_{nb}),$$
$$d_{W''} = \delta_{W''}\Delta\xi/(D_{W''} - \sum a_{nb}),$$
$$d_{P'} = \alpha_{P'}\Delta\eta/(D_{P'} - \sum a_{nb}),$$
$$d_{S'} = \alpha_{S'}\Delta\eta/(D_{S'} - \sum a_{nb}).$$

The velocity correction equations are given by

$$U_{P''} = U^*_{P''} + d_{P''}(P'_P - P'_E).$$
$$U_{W''} = U^*_{W''} + d_{W''}(P'_W - P'_P),$$
$$(U_\xi)_{P'} = (U^*_\xi)_{P'} + d_{P'}(P'_P - P'_N),$$
$$(U_\xi)_{S'} = (U^*_\xi)_{S'} + d_{S'}(P'_S - P'_P).$$

Pressure is updated using the relation $P = P^* + P'$, where P^* is the guessed pressure distribution and U^*, U^*_ξ are the velocity components obtained from the momentum equations using P^* as the distribution of pressure.

All the discretized equations are solved by the line-by-line method using the Thomas algorithm. For the discretized momentum equations the off-line values are guessed using the same concept as described by Patankar,[6] but for the pressure correction equation Van Doormaal and Raithby's suggestion[9] is used. With Van Doormaal and Raithby's approximation for P'_E, equation (29) takes the form

$$[a_P - (\theta - 1)a_E]P'_P = a_S P'_S + a_N P'_N + a_W P'_W + a_E[(P'_E)^0 - (\theta - 1)(P'_P)^0] + B \tag{30}$$

when lines are swept in the direction of increasing η. Here θ is a relaxation parameter. The optimal value of θ depends upon the problem. In general $1 \leqslant \theta < 2$. This approximation for off-line values accelerates the rate of convergence considerably.

Local Nusselt number

From equation (18) the discrete values of the Nusselt number at the locations $\eta = 0, 1, 2, \ldots$ are given by

$$Nu = -4(L-\lambda)\left(\frac{2F+1}{F+1}H_n - (1+F)H_{n-1} + \frac{F^2}{F+1}H_{n-2}\right)\Big/(H_b \delta L_c \Delta\xi_n), \tag{31}$$

where

$$F = \Delta\xi_n / \Delta\xi_{n-1},$$

$$H_b = \frac{\delta(X)}{\delta(0)}\left[U_1 H_1 \Delta\xi_2 + (\Delta\xi_2 + \Delta\xi_3)U_2 H_2 + \cdots + (\Delta\xi_{n-1} + \Delta\xi_n)U_{n-1}H_{n-1} + U_n H_n \Delta\xi_n\right]$$

and

$$\Delta\xi_i = \xi_i - \xi_{i-1}, \quad i = 2, 3, \ldots, n.$$

RESULTS AND DISCUSSION

The computer code was thoroughly tested for flow through a straight channel before computing results for the wavy channel. Results for both the developing and fully developed regions in a sinusoidal wavy channel are presented in terms of computer-generated profiles in Figures 5–17. Computations were performed for a dimensionless wall amplitude $\lambda/L_c = 0{\cdot}1$, 0·2 and 0·25 and for $L/L_c = 1{\cdot}0$. The Prandtl number was fixed at 0·72, while the Reynolds number was varied from 100 to 500. Solutions were obtained for an isothermal wall only. The figures depict only the first few and the last two pitch lengths. Also, due to symmetry about the channel centreline, the figures show the various profiles in half of the flow domain only; computations were also performed only in half of the flow domain.

Non-uniform grid spacing was employed in both directions through the use of factors defining the ratio of adjacent mesh sizes in each direction. In the transverse direction the mesh size was taken to be smallest near the channel wall and largest near the centreline of the duct. The ratio of adjacent grid sizes and the number of grid points in the transverse direction were taken to be 0·98 and 20 respectively. A half control volume was taken at the channel entry and adjacent to the channel wall and the centreline in the ξ-direction. In the axial direction X the ratio of adjacent grid sizes was taken to be 1·015 with 46 grid points up to $X = 16$. Twelve more equidistant grid points were taken in the range $16 < X \leqslant 20$ so as to be able to apply easily the boundary conditions in the fully developed region. This discretization with 58×20 grid points was decided upon after considerable experimentation with accuracy of the solution and reasonable computer time in mind. About 50 iterations were required for $\lambda/L_c = 0{\cdot}1$ and 120 for $\lambda/L_c = 0{\cdot}25$.

Figures 5–8 show the behaviour of the dimensionless velocity components U and V for dimensionless wall amplitude $\lambda/L_c = 0{\cdot}1$, $Re = 500$ and for $\lambda/L_c = 0{\cdot}25$, $Re = 100$ at various X-locations noted on the figures. Figures 9 and 10 depict the dimensionless velocity vector for the same parameters. It is observed that the negative V-component at the minimum cross-section and the positive V-component at the maximum cross-section increase with Re. This is due to the effect of fluid inertia on the velocity profiles.[3] Note also that in the diverging part of the channel the U-profiles are flattened at the centreline. From the distribution of U- and V-components of velocity it is apparent that the flow becomes more asymmetric in symmetrically lying cross-sections of the converging and diverging parts of the channel.

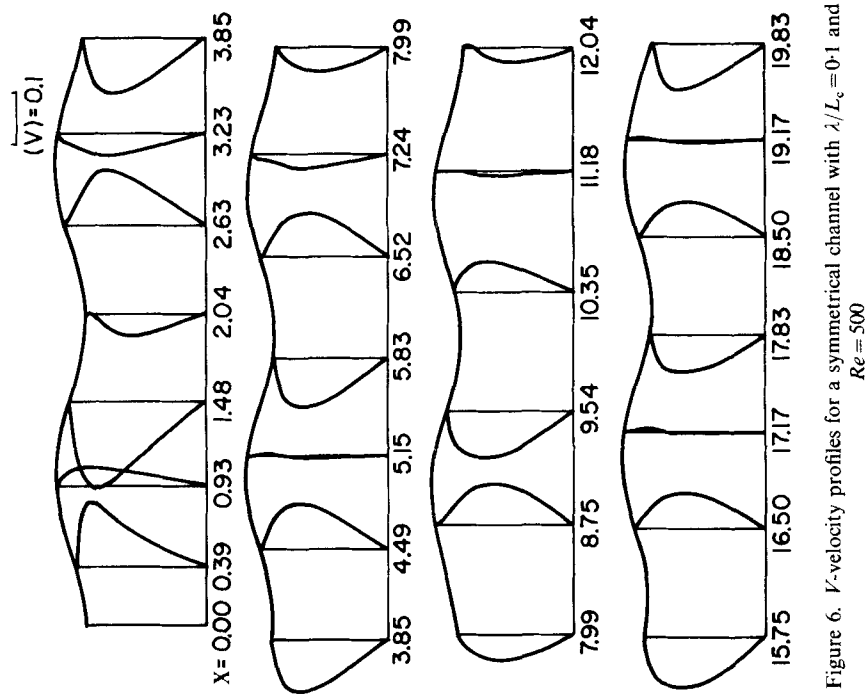

Figure 6. V-velocity profiles for a symmetrical channel with $\lambda/L_c = 0{\cdot}1$ and $Re = 500$

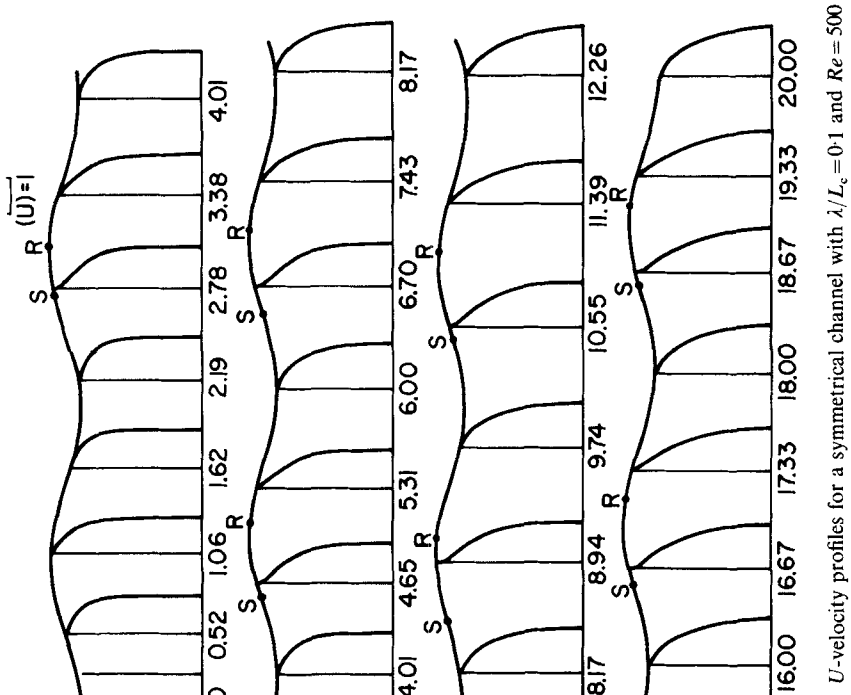

Figure 5. U-velocity profiles for a symmetrical channel with $\lambda/L_c = 0{\cdot}1$ and $Re = 500$

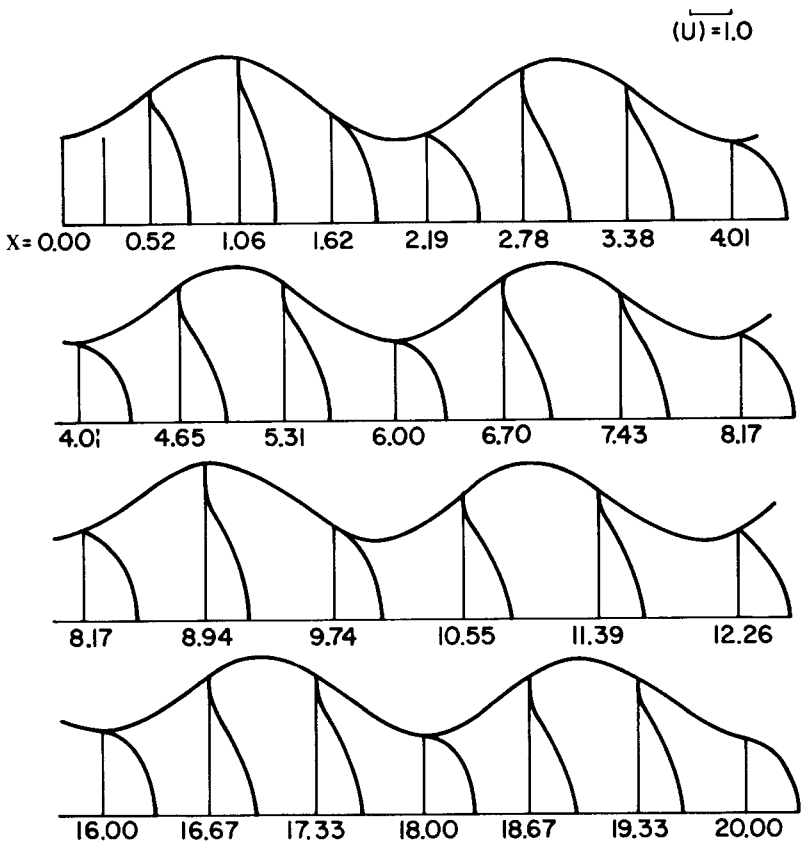

Figure 7. U-velocity profiles for a symmetrical channel with $\lambda/L_c = 0{\cdot}25$ and $Re = 100$

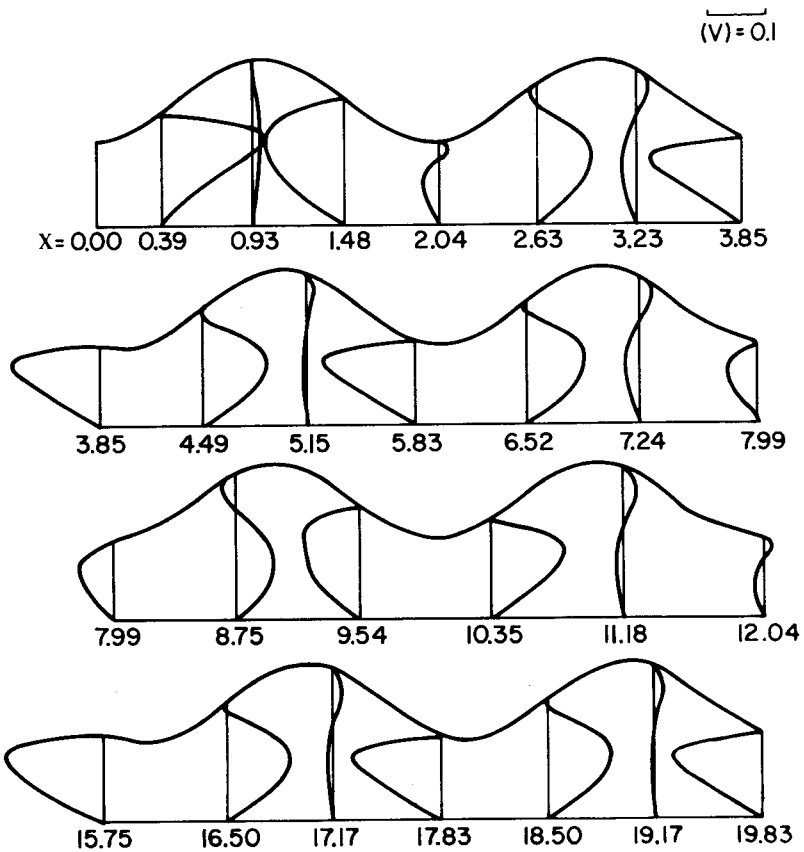

Figure 8. V-velocity profiles for a symmetrical channel with $\lambda/L_c = 0{\cdot}25$ and $Re = 100$

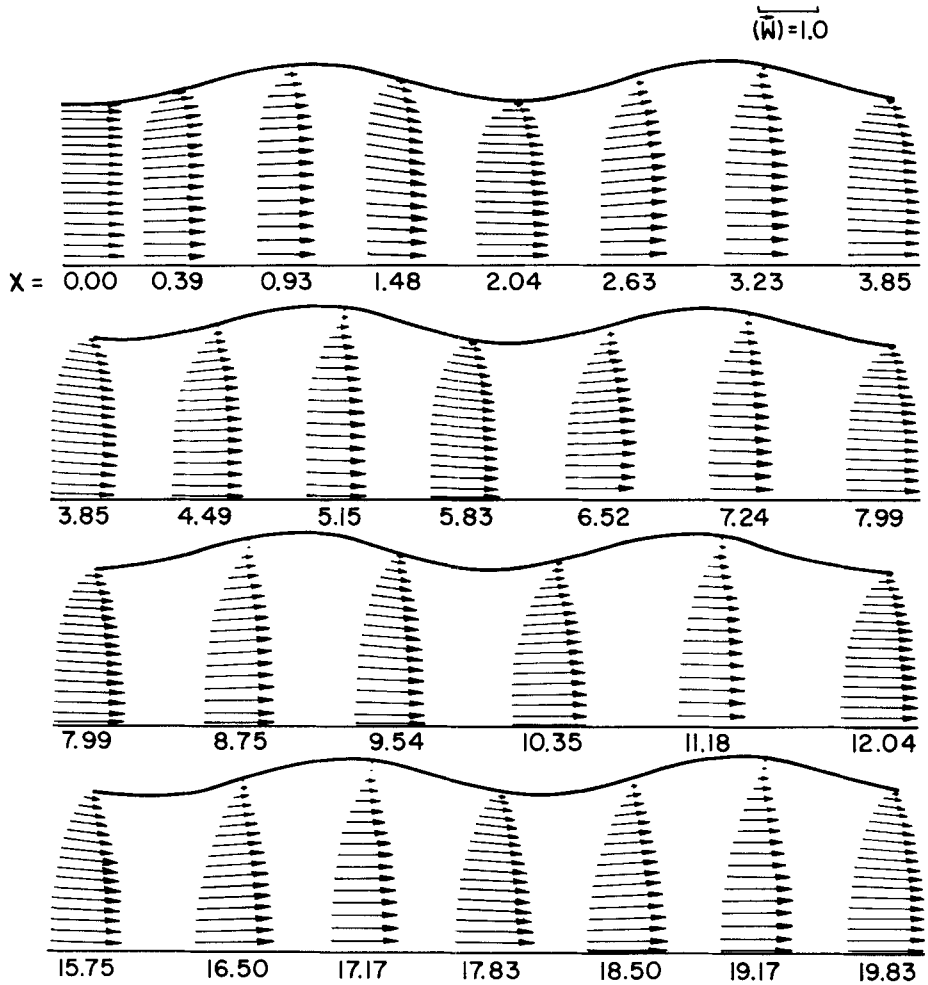

Figure 9. Velocity vectors in a symmetrical channel with $\lambda/L_c = 0{\cdot}10$ and $Re = 500$

It was found that for $\lambda/L_c = 0{\cdot}1$ and $Re = 100$ there is no separation of flow, but when Re is increased to 400 the flow begins to separate. From Figure 5 one finds a small backflow near the channel wall for $\lambda/L_c = 0{\cdot}1$ and $Re = 500$. The corresponding separation points (S) and reattachment points (R) are also shown in Figure 5. It was observed that as Re increases, the separation point moves upstream and the reattachment point moves downstream. The separated flow region grows not only with Re but also with the wall amplitude. From Figure 13 it is evident that for $\lambda/L_c = 0{\cdot}2$ and $Re = 500$ the backflow becomes stronger as well as more extensive. Moreover, for higher λ/L_c and Re separated flow occurs in the converging portion of the channel as well.

Figures 11 and 12 depict the behaviour of the dimensionless fluid enthalpy for the same combination of λ/L_c and Re values. From these figures we note that as the wall amplitude increases, the difference between the fluid enthalpy at the centreline and that at the wall decreases substantially. A similar effect can also be observed for a decrease in Re. Of these two parameters, the non-dimensional parameter λ/L_c has the stronger effect in reducing this difference. From a

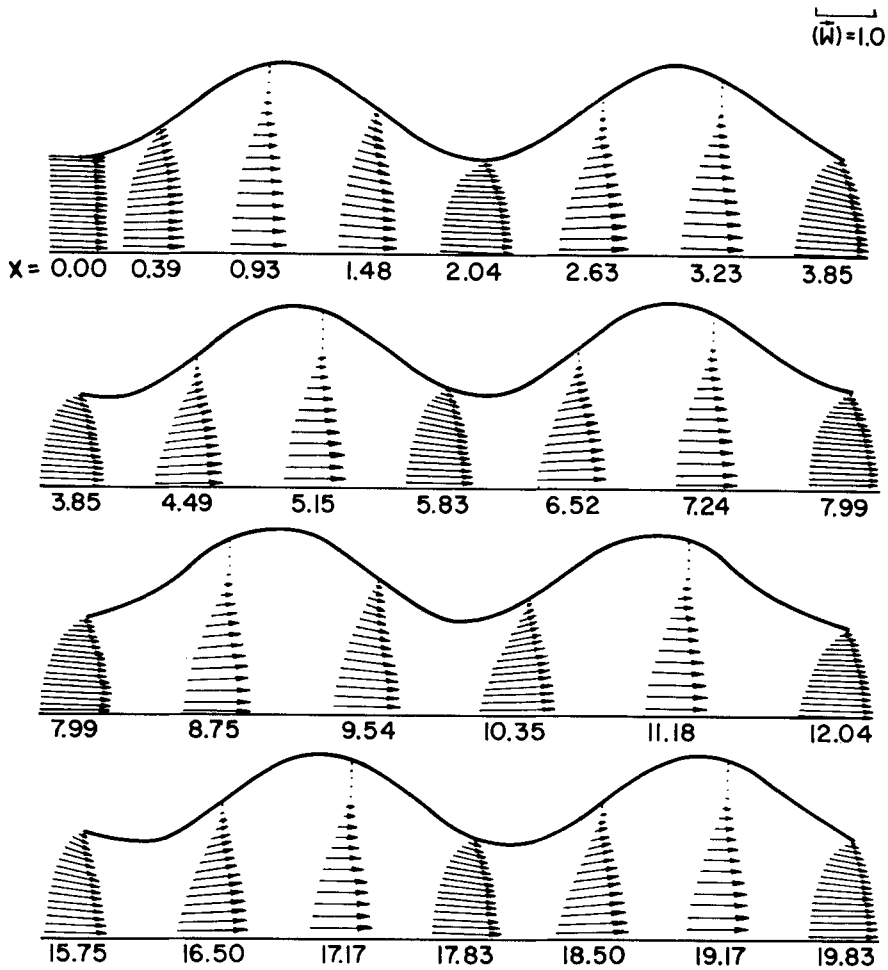

Figure 10. Velocity vectors in a symmetrical channel with $\lambda/L_c = 0{\cdot}25$ and $Re = 100$

careful inspection of the same figures it is seen that a point of inflection appears in the enthalpy profiles in the separated region, whereas in the non-separated region the enthalpy profile is almost parabolic.

Figures 14 and 15 show the dimensionless pressure distribution in the downstream direction for the same λ/L_c and Re values. It is possible to express this distribution as

$$P(X) = -f(X) + f'(X),$$

where $f'(X)$ behaves in a periodic fashion from cycle to cycle and $f(X)$ is linear in the fully developed region and nearly linear in the developing region. In a channel with straight walls $f'(X) = 0$ and $f(X)$ is linear in the fully developed region. The per-cycle pressure drop ΔP in the fully developed region is constant for each cycle but increases with an increase in wall amplitude. The variation of pressure in the Y-direction is negligible and has therefore not been shown.

Figures 16 and 17 depict the variation of local Nusselt number for the same values of λ/L_c and Re. While the Nusselt number is constant in a straight channel, it is larger and varies almost

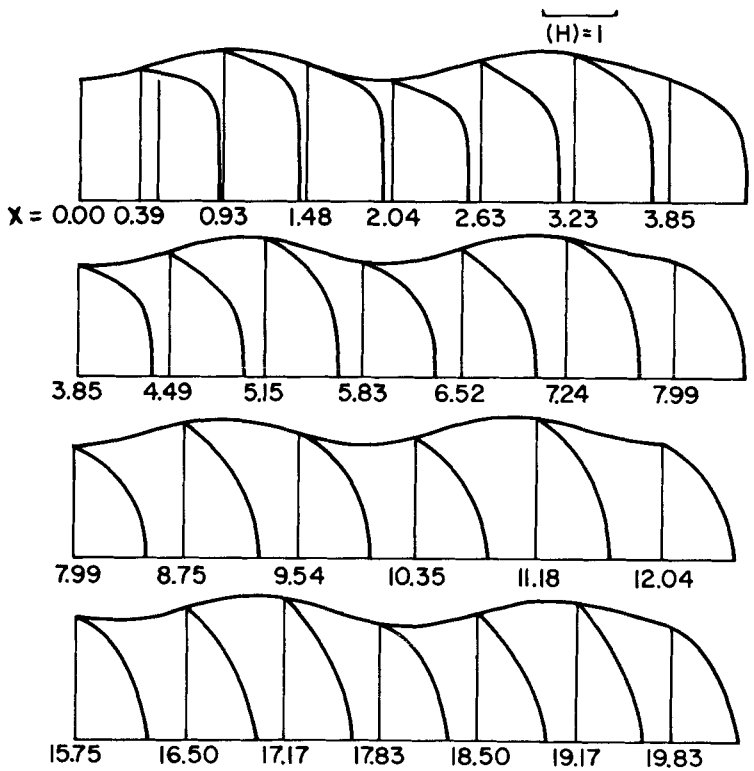

Figure 11. Enthalpy profiles for a symmetrical channel with $\lambda/L_c = 0{\cdot}1$ and $Re = 500$

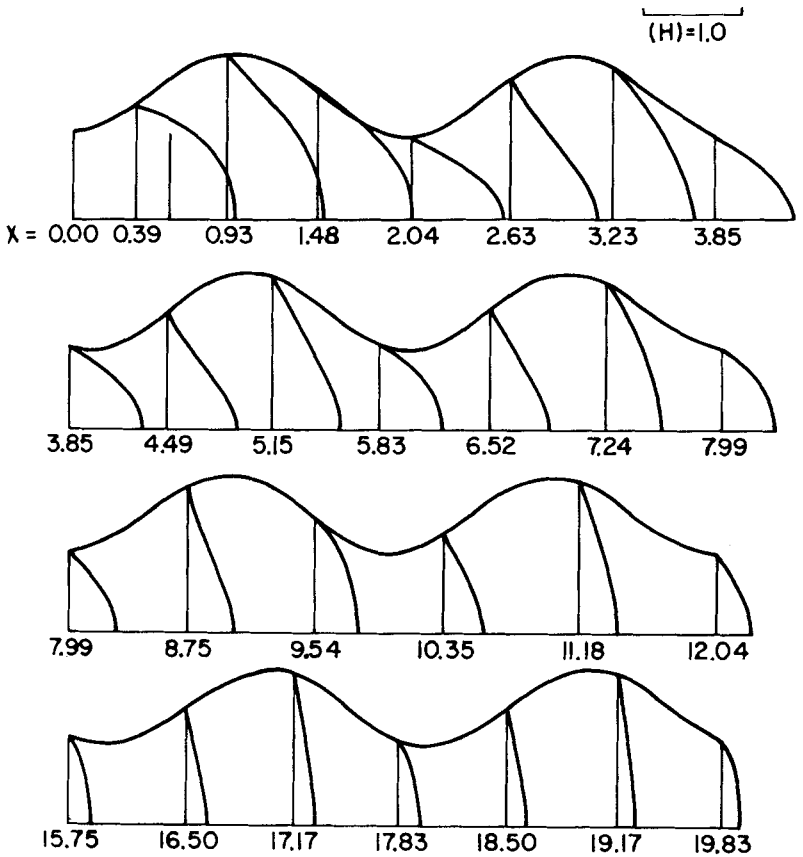

Figure 12. Enthalpy profiles for a symmetrical channel with $\lambda/L_c = 0{\cdot}25$ and $Re = 100$

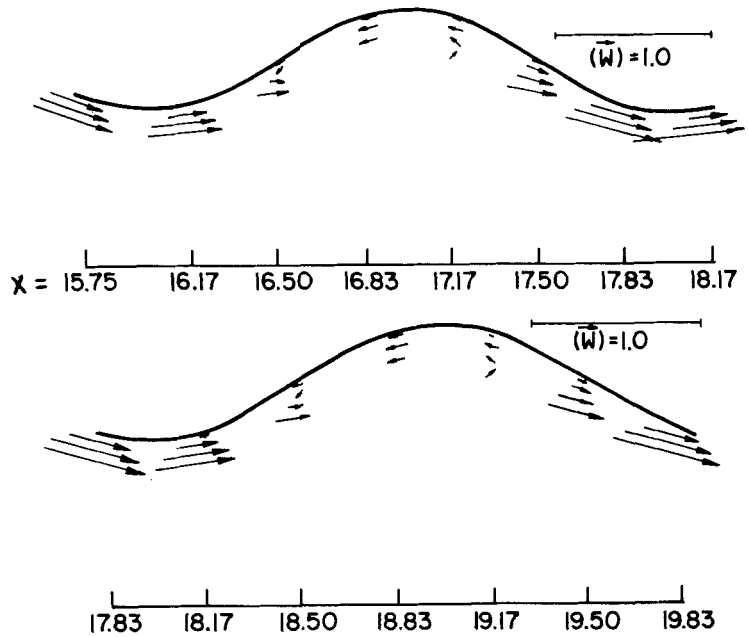

Figure 13. Velocity vectors in a symmetrical channel with $\lambda/L_c = 0{\cdot}2$ and $Re = 500$

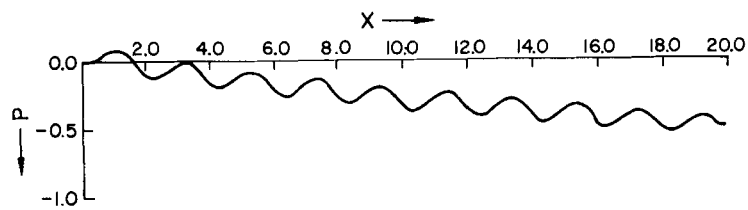

Figure 14. Centreline pressure distribution along X for a symmetrical channel with $\lambda/L_c = 0{\cdot}1$ and $Re = 500$

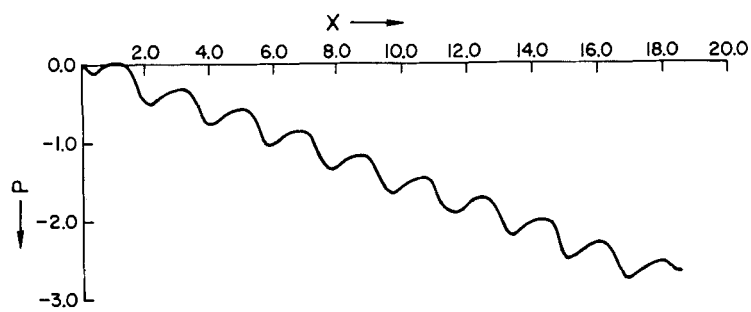

Figure 15. Centreline pressure distribution along X for a symmetrical channel with $\lambda/L_c = 0{\cdot}25$ and $Re = 100$

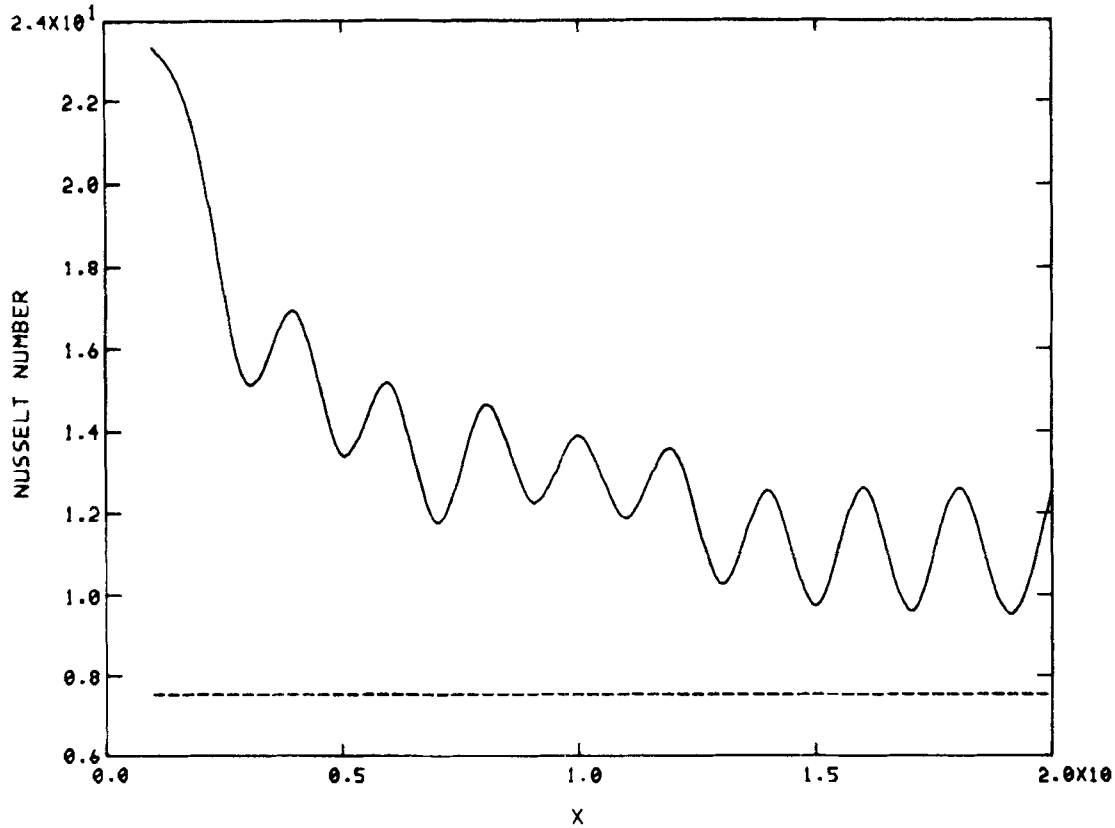

Figure 16. Variation of Nusselt number with X for $Re = 500$ and $\lambda/L_c = 0{\cdot}1$.

sinusoidally in a wavy channel and increases with Re. As expected, the Nusselt number is larger at the minimum cross-section and smaller at the maximum cross-section. The dashed line on these figures represents the constant value (7·54) of the Nusselt number for fully developed flow in a straight channel with isothermal walls.

CONCLUSIONS

A numerical solution for the laminar viscous flow with heat transfer in a sinusoidally curved converging–diverging channel has been obtained using body-fitted co-ordinates. Results found for a fixed Pr and L/L_c but for various values of Re and λ/L_c show the following:

The flow separates mainly in the diverging portion, but for higher Re and λ/L_c it separates in the converging portion as well. A point of inflection is observed in the enthalpy profiles in the separated region, whereas in the non-separated region this distribution is almost parabolic. Due to the effect of inertia,[3] the negative V-component of velocity at the minimum cross-section and the positive V-component at the maximum cross-section increase with Re. The pressure variation in the Y-direction is negligible, while in the axial direction it is a combination of a nearly linear and periodic variation. Per-cycle pressure drop in the fully developed region is constant for each cycle and increases with Re and λ/L_c. The Nusselt number varies sinusoidally and increases with the Reynolds number, unlike that in a straight channel.

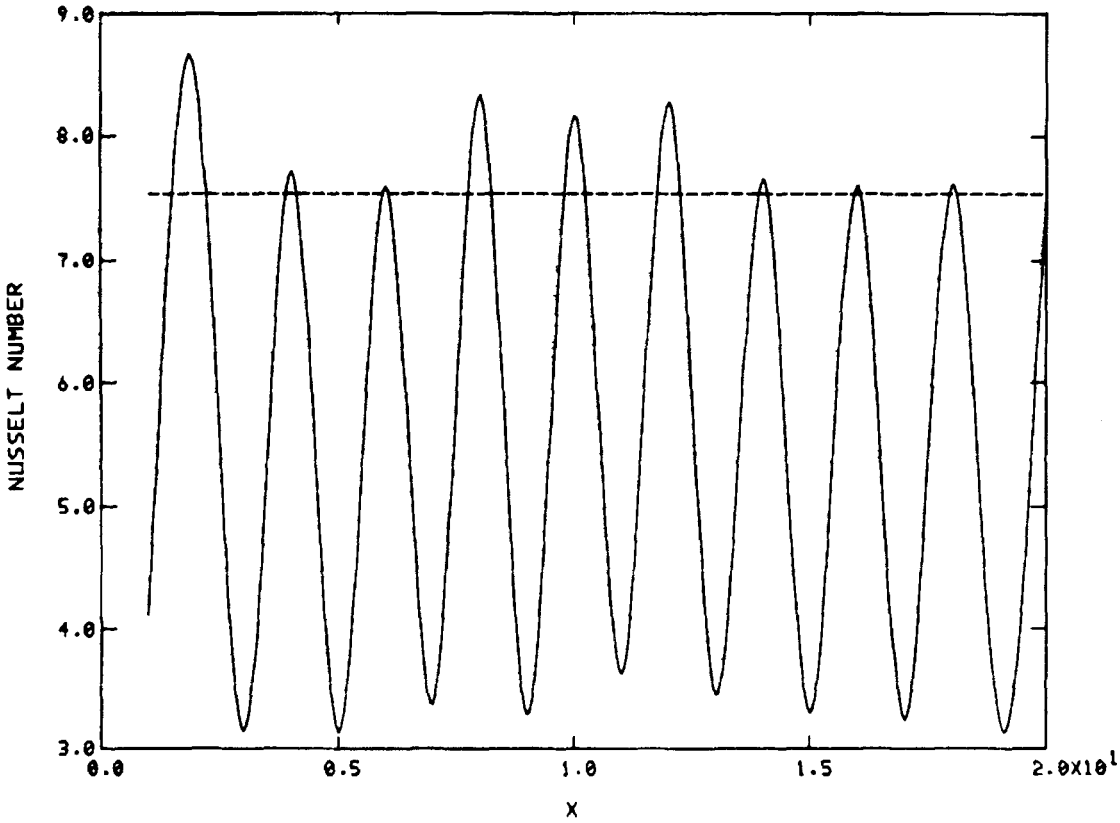

Figure 17. Variation of Nusselt number with X for $Re = 100$ and $\lambda/L_c = 0{\cdot}25$

ACKNOWLEDGEMENTS

This work was supported in part by a research grant from the Aeronautics Research and Development Board, Government of India. Support provided to the first author by The Ohio State University is also gratefully acknowledged.

REFERENCES

1. J. C. Burns and T. Parks, 'Peristaltic motion', *J. Fluid Mech.*, **29**, 405–416 (1967).
2. S. Tsangaris and E. Leiter, 'Analytical solutions for weakly-stenosed channels at low Reynolds numbers', *Proc. 1st Int. Conf. on Mechanics in Medicine and Biology*, 1978, pp. 289–292.
3. S. Tsangaris and E. Leiter, 'On laminar steady flow in sinusoidal channels', *J. Eng. Math.*, **18**, 89–103 (1984).
4. K. Vajravelu, 'Fluid flow and heat transfer in horizontal wavy channels', *Acta Mec.*, **35**, 245–258 (1980).
5. A. T. Prata and E. M. Sparrow, 'Heat transfer and fluid flow characteristics for an annulus of periodically varying cross section', *Numer. Heat Transfer*, **7**, 285–304 (1984).
6. S. V. Patankar, *Numerical Heat Transfer and Fluid Flow*, Hemisphere, Washington DC, 1980.
7. S. T. Hsu and J. F. Kennedy, 'Turbulent flow in wavy channels', *J. Fluid Mech.*, **47**, 481–502 (1972).
8. M. Faghri, E. M. Sparrow and A. T. Prata, 'Finite-difference solutions of convection–diffusion problems in irregular domains, using a nonorthogonal coordinate transformation', *Numer. Heat Transfer*, **7**, 183–209 (1984).
9. J. P. Van Doormaal and G. D. Raithby, 'Enhancements of the SIMPLE method for predicting incompressible fluid flows', *Numer. Heat Transfer*, **7**, 147–163 (1984).
10. M. E. Braaten and W. Shyy, 'Comparison of iterative and direct solution methods for viscous flow calculations in body-fitted co-ordinates', *Int. j. numer. methods fluids*, **6**, 325–349 (1986).